J. Fluid Mech. (1994), *vol.* 277, *pp.* 109–134

Particle response and turbulence modification in fully developed channel flow

By J. D. KULICK, J. R. FESSLER AND J. K. EATON
Department of Mechanical Engineering, Stanford University, Stanford, CA 94305, USA

(Received 15 October 1993 and in revised form 8 April 1994)

The interactions between small dense particles and fluid turbulence have been investigated in a downflow fully developed channel in air. Particle velocities of, and fluid velocities in the presence of, 50 μm glass, 90 μm glass and 70 μm copper spherical beads were measured by laser Doppler anemometry, at particle mass loadings up to 80%. These particles were smaller than the Kolmogorov lengthscale of the flow and could respond to some but not all of the scales of turbulent motion. Streamwise mean particle velocity profiles were flatter than the mean fluid velocity profile, which was unmodified by particle loading. Particle velocity fluctuation intensities were larger than the unladen-fluid turbulence intensity in the streamwise direction but were smaller in the transverse direction. Fluid turbulence was attenuated by the addition of particles; the degree of attenuation increased with particle Stokes number, particle mass loading and distance from the wall. Turbulence was more strongly attenuated in the transverse than in the streamwise direction, because the turbulence energy is at higher frequencies in the transverse direction. Streamwise turbulence attenuation displayed a range of preferred frequencies where attenuation was strongest.

1. Introduction

The interactions between turbulent flows and particles comprise a large number of interdependent effects, many of which remain poorly understood. In particular, the regime of particle-laden flows wherein particles have sufficiently small inertia to respond to some of the fluid velocity fluctuations but are too massive to act as fluid elements offers a host of complexities to the researcher. At very low particle concentrations, the base flow is not affected by the presence of the particles – a circumstance known as 'one-way coupling'. Conversely, 'two-way coupling' occurs if the particles carry a moderate fraction of the flow's mass and in turn modify the flow. The response of particles to a turbulent flow and the associated modification of turbulence by particles have been studied by researchers concerned with pneumatic conveyance, atmospheric transport of particulates, and pulverized coal and spray fuel combustion, among other applications. Nonetheless, there have been only a few well-qualified experimental measurements of particle–turbulence interaction in the sorts of simple flows required by turbulence model developers.

1.1. *Previous work*

Early investigations of particle-laden flow focused on the equation of motion of a single particle, particularly its coefficient of drag, and on the dispersion behaviour of a cloud of particles. The equation of motion of even a very small spherical particle has been shown to contain numerous force terms, including those due to viscous drag,

particle history, flow velocity gradients, particle spin and the proximity of a solid surface (see e.g. Maxey & Riley 1983).

Analytical treatments of particle dispersion tend to be complicated, and generally have been restricted to idealized cases of isotropic turbulence and very small particles. Starting with the work of Tchen (1947), most built on the diffusion theory of Taylor (1921). Yudine (1959) and Csanady (1963) examined the effects of particle inertia and body forces, and described the 'crossing-trajectories effect' whereby a particle under the influence of a body force is swept through turbulent eddies and thereby experiences a different range of turbulence states than does a fluid element. This effect reduces particle dispersion compared with turbulent diffusion. Snyder & Lumley (1971) and Wells & Stock (1983) measured inertial particle dispersion in decaying grid turbulence, and showed that the velocities of heavy particles decorrelate more quickly than do light particles. More recently, Squires & Eaton (1991) and Elghobashi & Truesdell (1992) performed direct numerical simulation of particle dispersion in isotropic turbulence, and found good agreement with prior theoretical and experimental studies. This confluence of computational, analytical and empirical results suggests that particle dispersion – in simple flows – is fairly well understood.

In contrast to particle dispersion, the response of particle velocities to turbulent fluctuations in fluid velocity is difficult to predict. In the absence of the crossing-trajectories effect the r.m.s. particle fluctuating velocity has been shown to be less than the turbulence intensity, in homogeneous turbulence. In an inhomogeneous turbulent flow with drifting particles, however, the local particle velocity fluctuation intensity is a function both of inertial response to local turbulent fluctuations and of a particle's velocity history, so that the particle velocity fluctuation intensity can be larger than the turbulence intensity, as shown by Soo (1956) and Liljegren (1993).

Particle-laden pipe flows are important in the pneumatic conveyance and process industries. Despite the very large number of studies of such flows, only a few quantities of interest have been measured extensively. Nearly all such experiments have found that the streamwise particle mean velocity profile is flatter than the corresponding fluid velocity profile, with particles leading the flow near the wall and lagging the flow in the core. This effect has been attributed to the transverse mixing of particles that, owing to their greater inertia, retain longer memories of their streamwise velocity than do fluid elements. Many of these same experiments showed that particle velocity fluctuation intensities were higher than the turbulence intensity, while others found the opposite case to obtain. Particles have been found both to raise and to lower the pressure drop, and there are no reliable means of predicting either the direction or the magnitude of the change based on particle and flow properties. (See Kulick, Fessler & Eaton, 1993 for an extensive review of the pipe flow literature.) The model development of Sommerfeld (1992) has shown that very small changes in the modelling of particle–wall collision dynamics can effect profound changes in particle velocity statistics elsewhere in the flow, which may account for the variations between experiments using different particle and pipe materials.

At sufficiently high mass loading (the ratio of particle mass flux to fluid mass flux) particles can modify fluid turbulence. Experiments with solid particles in air – where high mass loadings can be attained with a very small volume fraction of particles – have shown that small particles tend to attenuate turbulence while large particles augment turbulence. Such experiments have been performed in vertical pipe flows by Maeda, Hishida & Furutani (1980) and Tsuji, Morikawa & Shiomi (1984); in a vertical boundary-layer flow by Rogers & Eaton (1991); and in direct numerical simulation (DNS) of isotropic turbulence by Squires & Eaton (1990*b*) and Elghobashi & Truesdell

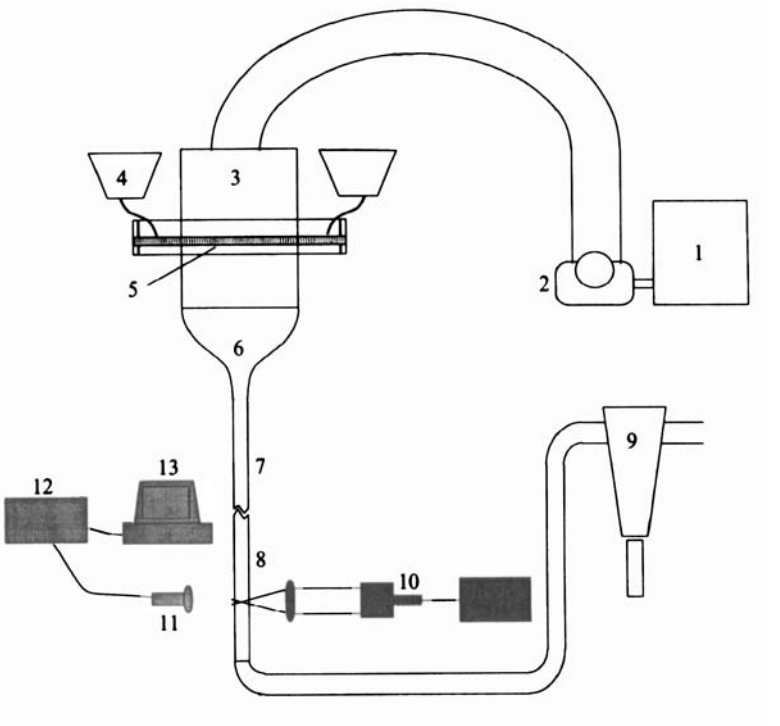

FIGURE 1. Wind tunnel schematic: 1, intake and seeding; 2, blower; 3, flow conditioning; 4, particle hopper; 5, belt feeder; 6, 10:1 contraction; 7, development section; 8, test section; 9, cyclone separator; 10, LDA transmitting optics; LDA receiving optics; 12, counter processor; 13, 386 computer.

(1993). These experiments are insufficient to characterize turbulence modification in a general flow because of the large number of important parameters in particle-laden turbulence: particle diameter, particle Stokes number, particle Reynolds number, particle/fluid density ratio, flow structure, flow direction and presence of walls. Results from these and other experiments in particle-, droplet- and bubble-laden jet and pipe flows have been surveyed in Gore & Crowe (1991), who showed that whether given particles increase or decrease turbulence intensity depends on the ratio of particle diameter to a characteristic eddy diameter of the turbulence. There is no further collapse of the data, however; the *degree* of turbulence modification does not depend in an obvious fashion on any simple set of parameters.

1.2. *Objectives*

The objective of this study was to investigate how small particles respond to turbulence in a shear flow and how turbulence is modified by particles, and to provide baseline data for development and testing of turbulence models. Particle-laden flows are, in general, characterized by a large parameter space. This study considered the effects of variations in particle Stokes number (ratio of particle relaxation time to fluid timescale) and particle mass loading, as well as variations through the boundary layer. Experiments were conducted in a turbulent channel flow, at $Re = 13800$ based on the channel half-width of 2 cm and centreline velocity of 10.5 m s^{-1}. These results have been compared with those of prior investigations and with some turbulence models.

2. Experimental facility and techniques

The experiments were conducted in a long vertical downflow wind tunnel. The tunnel was vertically oriented so that the gravitational force on the particles was aligned with the direction of flow, and was sufficiently long to ensure that the flow was hydrodynamically fully developed and that the particles were not accelerating at the measurement location. Particles were chosen to provide a range of Stokes numbers while being smaller than the Kolmogorov lengthscale of the turbulence. A specially designed particle feeder allowed an initially uniform distribution of particles at the entrance to the development section.

2.1. *Wind tunnel*

Figure 1 is a schematic illustration of the wind tunnel. The air intake, flow conditioning and particle feeding sections were mounted on a platform 7.6 m above the laboratory floor. The particle feeder was a specially designed system of belt-mounted buckets that were filled rapidly outside the tunnel, and which then drained slowly and uniformly as they were pulled through the tunnel, thereby ensuring uniform loading in the transverse direction. Subsequent flow conditioning promoted spanwise mixing of particles.

At the exit of the contraction, a honeycomb cell prevented particles from being thrown towards the tunnel centreline. Boundary-layer trips were affixed to both walls at the entrance to the 5.2 m long, 4.0 cm × 45.7 cm particle board development section. Pressure taps were located along the centreline of one wall, for measuring the streamwise pressure gradient. The 63.5 cm long acrylic test section had a removable panel that allowed cleaning the walls and swapping panel inserts for flow visualization and hot-wire measurements. The flow exited the test section into a cyclone separator, where the particles were collected for re-use. The cyclone separator imposed a higher operating pressure on the tunnel – 1.5 kPa above atmospheric – than would occur in a conventional facility of the same dimensions.

2.2. *Particles*

Three classes of spherical particles were used in these experiments (see table 1). The 50 and 90 μm glass beads were aerodynamically classified into nominally ± 5 μm windows, and the 70 μm copper shot was sieved into a ± 10 μm window. The corrected particle relaxation time, τ_p, was found by integrating the equation of motion for a particle with $Re_p < 100$ (see Kulick *et al.* 1993) in free fall in an unbounded fluid, and determining the time required for the particle to come to 63% of its terminal velocity. The Stokes number, St_f, is based on the corrected particle relaxation time and the turbulence timescale, k/ϵ, at the channel centreline.

2.3. *Measurement apparatus and techniques*

A single-component forward-scatter laser Doppler anemometer (LDA) allowed measurements of the streamwise and transverse components of the airflow and particle velocity. The system incorporated a 35 mW Helium-Neon laser and two TSI 1980 counter processors; data were acquired and processed on a 386SX personal computer. Nominally 1 μm titanium dioxide powder was used as a flow tracer.

Two orientations of the optical path were used for streamwise measurements, and one for transverse measurements. At low mass loadings, streamwise velocities were measured with the LDA optical axis oriented in the spanwise direction. This alignment allowed excellent spatial resolution, because the direction of the mean fluid velocity

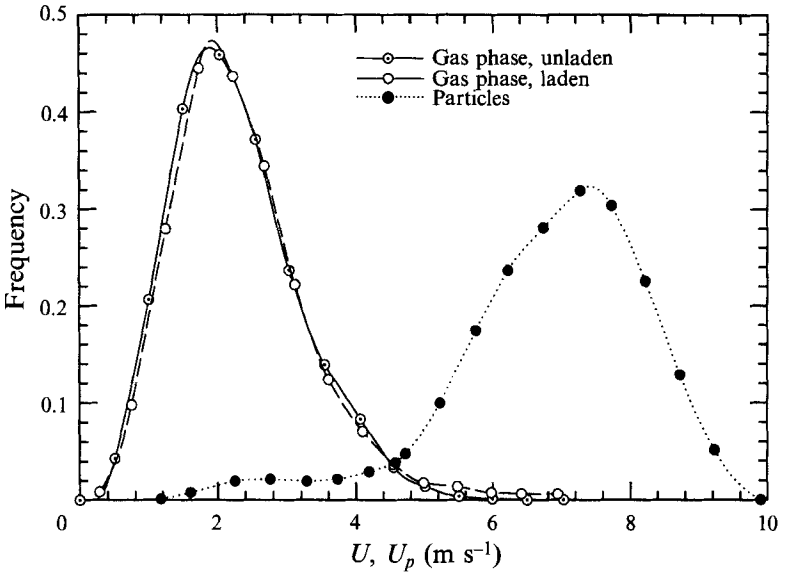

FIGURE 2. Qualification of LDA phase discrimination.

Material	Glass	Glass	Copper
Density (kg m^{-3})	2500	2500	8800
Nominal diameter (μm)	50	90	70
Mass-weighted mean diameter (μm)	53.2	92.3	69.6
Stan. dev. of diameter (μm)	3.1	4.5	10.9
Stokes τ_p (ms)	19	63	130
Corrected τ_p (ms)	18	43	95
Still-air terminal velocity (m s^{-1})	0.18	0.42	0.93
St_f	0.57	1.4	3.0

TABLE 1. Particle properties

gradient was along a minor axis of the elliptical LDA measurement volume (which was 78 μm in diameter and 562 μm in length). At higher mass loadings, however, the particles obscured the relatively long path between the measurement volume and the receiving optics, giving an unacceptably low signal-to-noise ratio. In these cases, the optical axis was oriented in the transverse direction, which provided a much shorter optical path but poorer near-wall spatial resolution.

Particle velocities were measured in the conventional fashion, with the LDA seed turned off. Gas-phase velocities in particle-laden flows were distinguished from particle velocities by means of amplitude discrimination. This method exploits the large difference in amplitude between Doppler burst pedestals in light scattered from large inertial particles and from small flow tracers. By setting the amplitude-discrimination threshold accordingly, only those Doppler bursts with small pedestal amplitude were validated. Figure 2 shows particle and fluid streamwise velocity probability density functions (PDFs) at a location in the flow where the mean relative particle velocity was large, demonstrating the minimal interphase cross-talk. The absence of cross-talk was confirmed at each measurement point by comparing the data rates for gas-phase measurements with and without the LDA seed; data rates typically increased a hundred-fold when the seed was added.

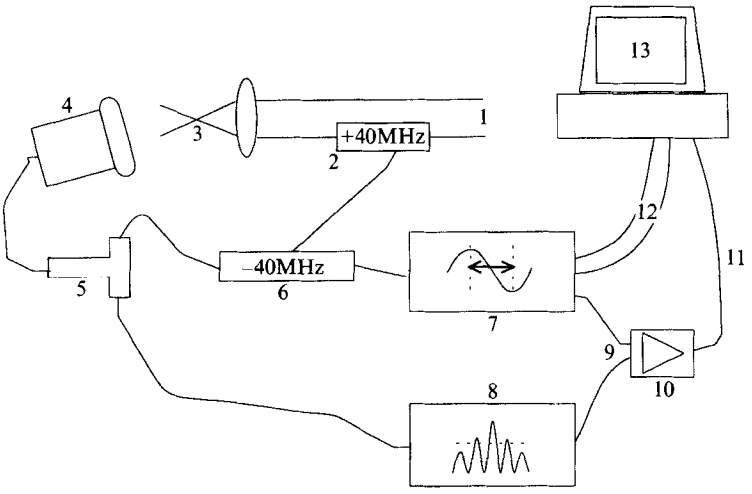

FIGURE 3. Two-counter method schematic: 1, laser beams; 2, Bragg cell; 3, measurement volume; 4, receiving optics; 5, power splitter; 6, frequency shifter; 7, amplitude counter; 8, data counter; 9, 'data ready' lines; 10, 'data ready' validation circuit; 11, validated 'data ready' line; 12, Doppler frequency digital lines; 13, 386SX computer.

Transverse gas-phase velocities could not be measured in laden flow with the aforementioned technique, as the frequency shifter used with the Bragg cell removed the pedestal from the photodetector output. The Bragg cell shifts the frequency of one beam – and hence the Doppler frequency – by 40 MHz. The frequency shifter high-pass filters the photodetector output at 25 MHz, thereby removing the pedestal component, before applying a 39 MHz shift for an effective 1 MHz shift of the signal at the input to the counter processor. A novel circuit was devised to surmount this difficulty, using two counter processors (see figure 3). One counter processor (the 'data counter') received the downmixed signal and determined the Doppler frequency; the other ('amplitude counter') received the raw photodetector output. The 'cycles/burst' control of the amplitude counter was set to 2, so that Doppler bursts were validated entirely on the basis of pedestal amplitude. The 'data ready' output lines of both processors were then compared by a temporal coincidence circuit; if both lines were raised within a 100 μs window, then they were deemed to have signalled the same event and the burst was validated. The 'two-counter' technique was qualified by measuring streamwise velocities and comparing with conventional measurements at the same location; the results are shown in figure 4.

Gas-phase data rates were typically about 2000 Hz when measuring unladen flow velocities, and varied from 3000 Hz at low particle mass loadings to 100 Hz at the highest mass loadings. Particle velocity data rates increased with mass loading, varying from 20 to 400 Hz. When making spectral measurements the LDA seed flow rate was set at its maximum, and laden-flow gas-phase data rates up to 6000 Hz were attained.

Since flow-tracer particles arrive at the measurement volume at random times, power spectra of the gas-phase velocity could not be measured in the conventional fashion, which requires a periodically sampled velocity signal. The present study used the method of Gaster & Roberts (1977), which computes the power spectrum by Fourier transforming the autocovariance of the sampled data. The autocovariance was formed using 150000 samples.

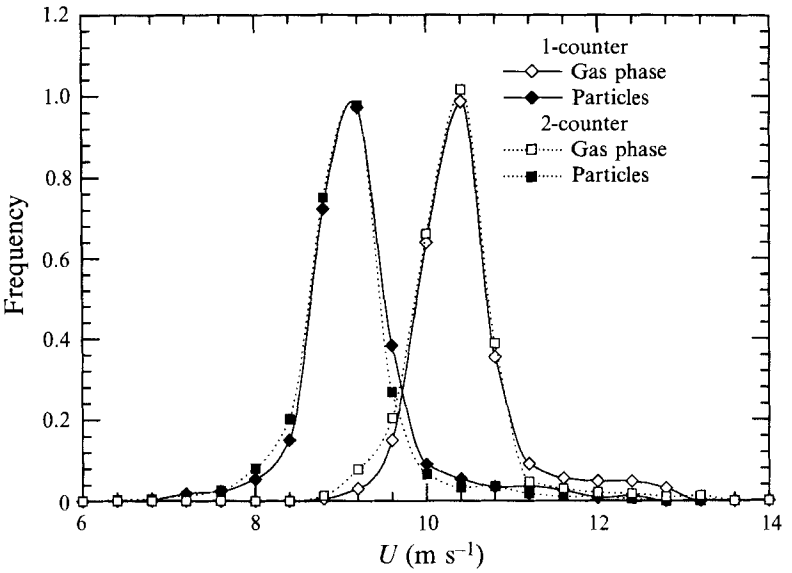

FIGURE 4. Qualification of two-counter phase discrimination.

2.4. *Experimental uncertainty*

The combined experimental uncertainty due to directional bias, gradient broadening, velocity bias, ensemble statistical errors and alignment uncertainty was estimated at 2% in the mean velocity and 5% in the standard deviation (see Kulick *et al.* 1993). The uncertainty in the gas-phase velocity due to interphase cross-talk was estimated at 1% in the mean and up to 3% in the standard deviation. (Note that cross-talk error can serve only to *increase* the measured gas-phase turbulence intensity.) For particle velocities, the variance in particle diameter resulted in a deviation from idealized behaviour that is not properly denoted as measurement uncertainty. The variance in particle terminal velocity associated with the variance in diameter introduced apparent standard deviations in particle velocity of approximately 3 cm s^{-1} for the 50 and 90 μm glass particles and 20 cm s^{-1} for the 70 μm copper particles.

3. Presentation and discussion of results

All experiments were run at a centreline air velocity of 10.5 m s^{-1}, corresponding to a Reynolds number of 13800 based on channel half-width. Measurements of the streamwise pressure gradient yield a shear velocity, u_τ, of 0.49 m s^{-1}. As is shown below, the gas-phase mean velocity profile is unchanged by the presence of particles, so this condition corresponds to a constant mass flow of air. In the interest of brevity, no data are reported from experiments with 90 μm glass particles. In all cases, these quantities and effects were intermediate to those with 50 μm glass and 70 μm copper particles.

3.1. *Particle response*

3.1.1. *Particle loading uniformity*

Special care was taken to ensure that the initial particle concentration and velocity profiles were uniform. Non-uniformity in particle loading can induce modifications to gas-phase mean velocity profiles, and thereby alter the rates of production of turbulence kinetic energy. More immediately, gas-phase mean velocities must be

known to determine particle slip velocities. In a downward flow the gravitational force on particles acts as a source of momentum to the gas phase. In regions of high particle concentration, therefore, flow velocities may be increased relative to their particle-free values. However, in a flow with strong velocity gradients and non-uniform particle slip velocities, uniform particle concentration does not necessarily correspond to uniform drag, and a distinction needs to be drawn between uniform particle concentration and uniform particle flux. If particle concentration were uniform across the channel, then the local drag force (per unit volume) D would be proportional (assuming Stokes drag) to the particle slip velocity,

$$D = \frac{C}{\tau_p}(\bar{V} - \bar{U}), \tag{1}$$

where C, V and U are the particle concentration (mass of particles per unit volume), particle velocity and fluid velocity, respectively, and where overbars denote averages. If particle slip velocity were uniform across the channel then the drag loading would be uniform as well. The experiments mentioned in §1.1 showed that slip velocities typically are not always uniform.

In the case of uniform particle mass flux, $\dot{m}_p$, the mean drag per unit volume from particles is

$$D_m = \frac{\dot{m}_p}{\tau_p}\left(\frac{\bar{V} - \bar{U}}{\bar{V}}\right). \tag{2}$$

Again considering the ideal case of uniform particle slip velocity, (2) shows that the drag force should increase as the wall is approached, because the drag force is inversely proportional to the particle velocity. The particle concentration also increases as the wall is approached because the mass flux of particles is constant while the mean convection velocity of the particles is decreasing. On these points, too, the literature shows no consistent trends.

It is difficult to determine, *a priori*, the uniformity of particle concentration and flux in the present experiments. Particles enter the development section with uniform concentration and flux. Flow velocities decrease near the walls as the boundary layers develop, increasing near-wall particle concentrations. Counteracting these tendencies is turbulent dispersion acting over a long development section. The shortest particle residence time relative to particle relaxation time is for a 70 μm copper particle in the centreplane: at a nominal speed of 10 m s^{-1} a particle would take approximately 0.5 s to reach the measurement location, or five relaxation times. Were there no transverse particle motions, this would be more than adequate time for a particle to come to its terminal velocity. With turbulent dispersion and wall reflections, however, this same time should be adequate for reducing particle concentration gradients by Fickian diffusion-like processes.

The degree of particle concentration non-uniformity could not be determined directly with the experimental instrumentation. Photographs of particle-laden flow in X–Y cross-section revealed no apparent mean concentration gradient when viewed in ensemble, but possible variations within the sublayer would not be resolvable. Without regard to the relative contributions of particle concentration and slip velocity, evidence that the effective drag loading was nearly uniform is provided by figures 5(*a*) and 5(*b*), which show gas-phase mean velocity profiles for varying particle size and mass loading. (In figure 5 and all subsequent velocity profiles, the value of u_τ used for normalizing to wall coordinates is the nominal value in the single-phase channel flow, 0.49 m s^{-1}.) For each set of particle conditions, the tunnel speed was adjusted so that the laden-flow

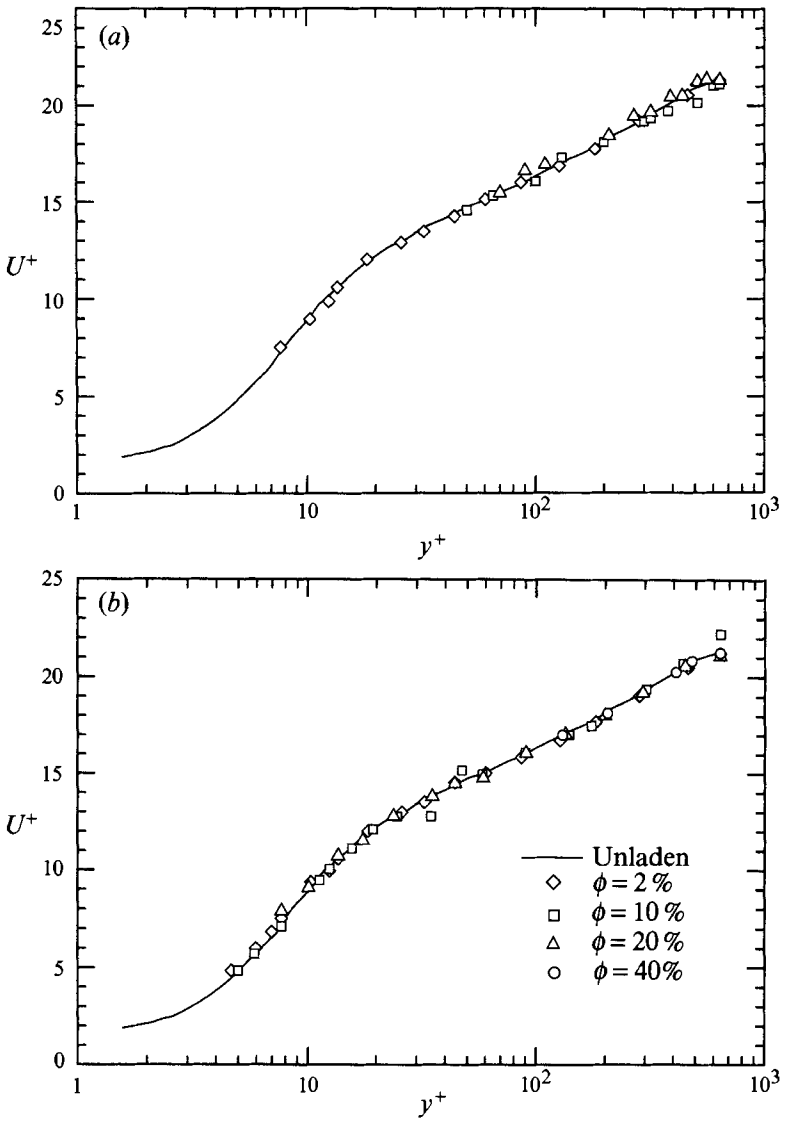

FIGURE 5. Gas-phase mean streamwise velocity profiles in the presence of (*a*) 50 μm glass particles; (*b*) 70 μm copper particles.

velocity matched the unladen-flow velocity at the centreline. Laden-flow mean velocities agreed with the reference profile to within the quoted experimental uncertainty, so there was no apparent modification to the mean flow. It should be noted, however, that as mass loading was increased and particle mass was decreased, near-wall measurements became more difficult. Consequently, at the high mass loadings that might be expected to modify the near-wall flow the most, no such measurements are available and so no conclusions may be drawn.

3.1.2. *Particle velocities*

Profiles of particle mean and r.m.s. fluctuating velocities in the streamwise and normal directions are presented and compared with the same quantities for the gas phase in the unladen reference flow. Each data point represents 2000 samples.

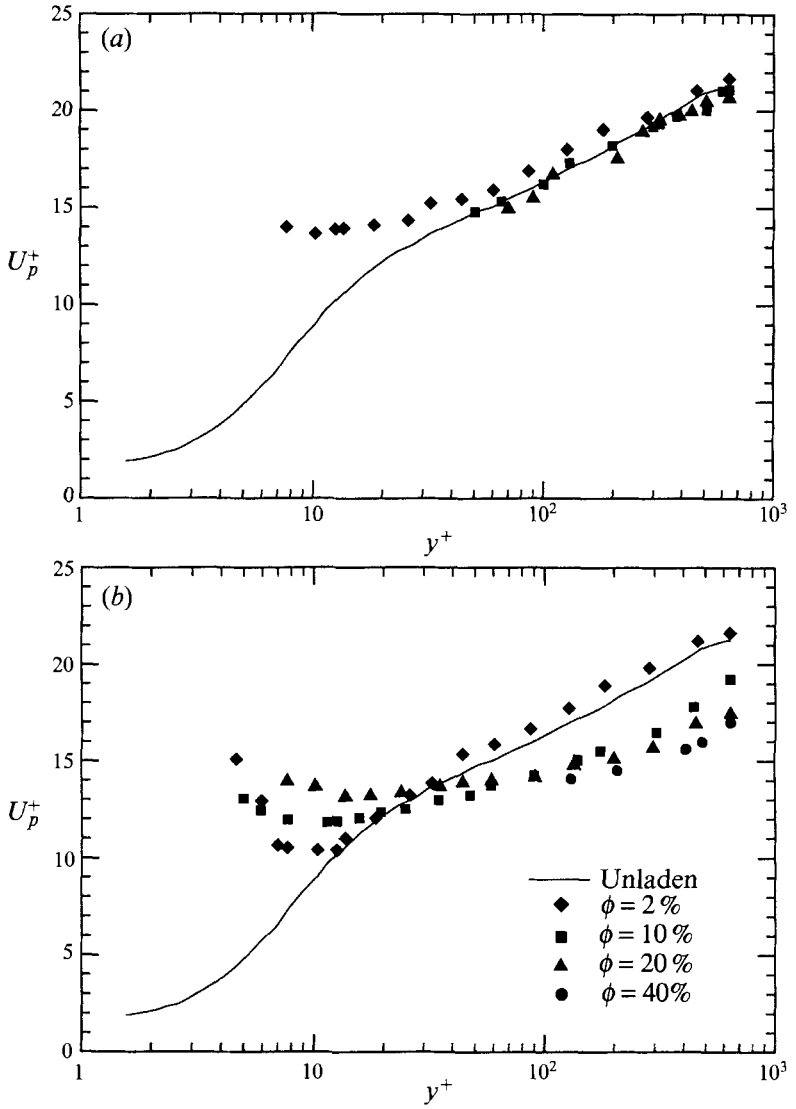

FIGURE 6. (*a*) 50 μm glass particle streamwise mean velocity profiles; (*b*) 70 μm copper particle streamwise mean velocity profiles.

Streamwise velocity profiles are presented in wall coordinates, with the normalizing wall shear stress taken from the gas-phase shear velocity for the reference flow. Fluctuation intensities are normalized by the gas-phase centreline velocity.

Figures 6(*a*) and 6(*b*) depict the variation of particle mean velocity with distance from the wall, Stokes number, and mass loading. Several features of these plots are worthy of note. The first is that particle velocity profiles are flatter than gas-phase profiles, so that slip velocities are substantial in the near-wall region where flow mean velocity gradients are steep. This effect decreases with increasing Stokes number. Moreover, particle velocities appear actually to *increase* near the wall, for those cases where they could be measured. This effect may be due to large normal fluctuating velocities of the particles. Assuming a linear velocity gradient, particle motions normal to the direction of the flow should not affect the mean streamwise velocity. However,

the situation is not symmetrical near the wall where high-speed particles moving toward the wall may hit the wall and rebound still carrying much of their streamwise momentum. Therefore particles crossing through a point in the viscous sublayer coming from either above or below may have a higher velocity than the local fluid velocity. One might expect that particle wall-normal velocity fluctuations would be strongly damped near the wall similar to fluid wall-normal fluctuating velocities. However, Rizk & Elghobashi (1985) have shown analytically that particles near the wall may have a much larger normal fluctuating velocity than the fluid. This analysis is somewhat borne out by the particle fluctuating velocity measurements presented below.

A second observation is that particle velocities decrease with increasing mass loading, except for the 70 μm particles inside $y^+ = 20$. The variation is small for the 50 μm glass particles, but is considerable for the 70 μm copper particles. Bearing in mind that the flow was oriented downward, then, as the particle Stokes number (and therefore terminal velocity) was *increased* particles increasingly lagged behind the flow. The terminal velocity of a single 70 μm copper particle is 0.95 m s^{-1}; in comparison, at a mass loading of 0.4 the mean slip velocity at the centreline was -2.2 m s^{-1}. The large change in the copper-particle mean velocity profiles with loading is difficult to explain. Simple analyses rule out a significant effect of inter-particle collisions. We believe that electrostatic effects may have contributed to this result. A large charge could have built up on the insulating Plexiglas walls, possibly causing the observed changes in the particle mean velocity profiles. The amount of charge accumulated on the walls would probably be a function of mass loading. Further experiments in channels fabricated from different materials or using different particles are needed to clarify this issue.

For the 50 and 90 μm glass particles, then, particle drag loading was uniform except perhaps very near the wall, where particle velocities exceeded gas velocities. For the 70 μm copper particles, assuming uniform particle concentration, drag loading would appear to increase with distance from the wall. This variation should then flatten the gas-phase velocity profiles, which does not occur to any appreciable extent. As the mean velocity gradients are unmodified, consideration of the fluid-phase momentum equation (Kulick *et al.* 1993) shows that either the pressure gradient or the Reynolds stresses must have changed to balance the drag loading. Unfortunately, neither of these quantities was measured; the single-component LDA did not allow Reynolds stress measurements, and heavy flows of LDA seed blocked the pressure taps so as to obviate reliable pressure readings. (As shown later, however, turbulence in both the streamwise and transverse directions was reduced by particles, and so it is likely that Reynolds stresses also were reduced. A reduction in Reynolds stress – in the absence of competing effects – would have caused the mean velocity profile to become more rounded. This effect may have counteracted the drag-induced flattening, for a zero net modification.)

Streamwise particle fluctuation intensities are displayed in figures 7(*a*) and 7(*b*). Figure 7(*a*) shows that, within the experimental uncertainty, 50 μm glass particles had nearly the same fluctuation intensity as the turbulence intensity. Figure 7(*b*) shows that the fluctuation intensity of the 70 μm copper particles increased with mass loading in the outer region and decreased in the inner. Given the greater variance in particle diameter for the heavier particles it is not surprising that measured velocity variances should increase with Stokes number near the centreline, even though larger particles are less responsive to turbulent fluctuations.

Two behaviours are difficult to explain, however. Figure 7(*a*) suggests that 50 μm glass particles acted as flow tracers – in at least a time-averaged sense – yet figure 6(*a*)

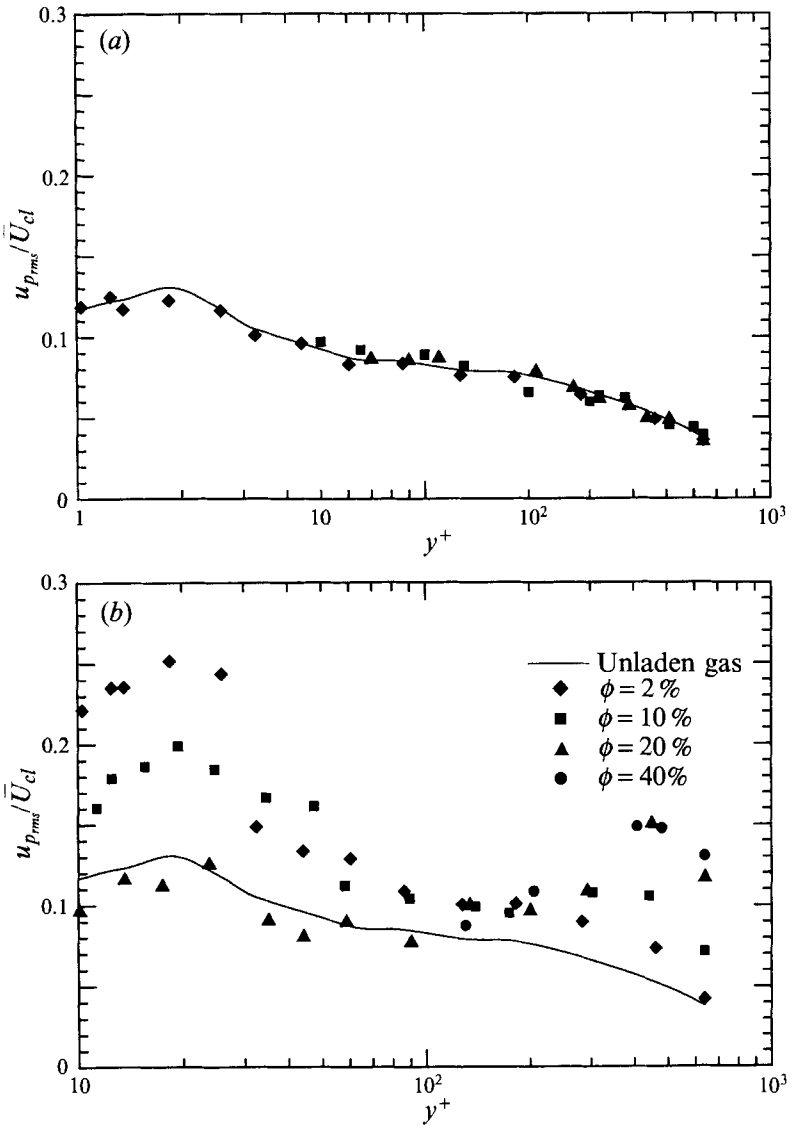

FIGURE 7. (*a*) 50 μm glass particle streamwise fluctuation intensity profiles; (*b*) 70 μm copper particle streamwise fluctuation intensity profiles.

shows that the particles had large slip velocities near the wall. The large values of near-wall fluctuation intensity for 70 μm copper particles can be misleading if interpreted as measures of the width of Gaussian velocity distributions. As can be seen from the velocity PDFs at $y^+ \approx 12$, shown in figure 8, near-wall particle velocity distributions were bimodal at these low mass loadings of 0.02 and 0.1, respectively. Of the two preferred velocity modes, one is characteristic of the outer region and one of the inner. Since these PDFs suggest that the local particle velocity variances are not due primarily to response to local turbulent fluctuations, it is curious to note that the peaks in fluctuation intensity are collocated with the peak in turbulence intensity in the reference flow. Also to be noted is that this location is the one at which mean slip velocities are zero (cf. figure 6*b*). It is possible that the two peaks reflect the different

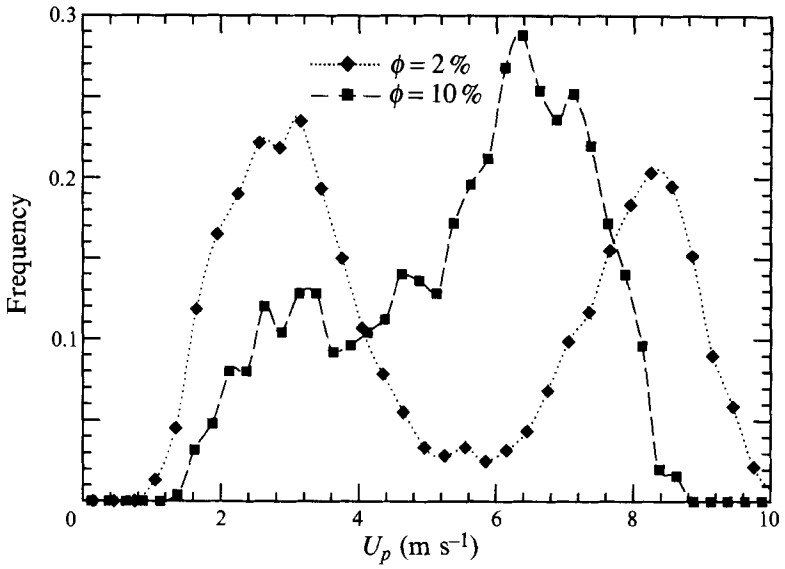

FIGURE 8. 70 μm copper particle streamwise velocity PDF at $y^+ = 12$.

velocities of incident and reflected particles; photographs of particle–wall impacts show them to be both infrequent and nearly elastic, with little loss of transverse momentum on rebound. Nonetheless, rebounding particles will, on average, have spent more time in the low-speed near-wall region than will incident particles at the same location, and will thus have lost more streamwise momentum to drag.

It remains unclear why this bimodality appears only at low mass loadings. A possible explanation is that the very-near-wall region (within several particle diameters) becomes saturated with particles as the mass loading increases. At low mass loadings, then, at a measurement location near the wall, the number of fast particles incident towards the wall is roughly the same as the number of slow particles that have been ejected after having been trapped in the viscous sublayer, with the resulting bimodal velocity PDF. At higher mass loadings the deposition rate increases, but the rate of accumulation of particles in the sublayer does not. Most incident particles therefore rebound immediately with only a small loss in streamwise momentum. While the rate of particle ejection remains constant as mass loading is increased, the fraction of particles at a given location that have been ejected decreases, and the PDF tends towards unimodality. None of the very-near-wall particle velocity and concentration measurements that would be necessary to verify this scenario could be acquired.

Profiles of transverse particle fluctuation intensity are exhibited in figures 9(*a*) and 9(*b*). These data suffer from greater scatter than do the corresponding streamwise measurements, but several trends are apparent. Fluctuation intensities are smaller than flow turbulence intensities. Furthermore, fluctuation intensity decreases and profile flatness increases with increasing Stokes number, and fluctuation intensity generally decreases with mass loading. Although particles are not subject to a kinematic constraint that velocities be zero at the wall, particle velocity fluctuations are seen to tend to zero with the turbulence intensity in figure 9(*b*).

Several factors contribute to transverse fluctuation intensities being smaller than turbulence intensities, while streamwise fluctuation intensities generally are larger. First, the variance in particle terminal velocity has no effect on measured velocity

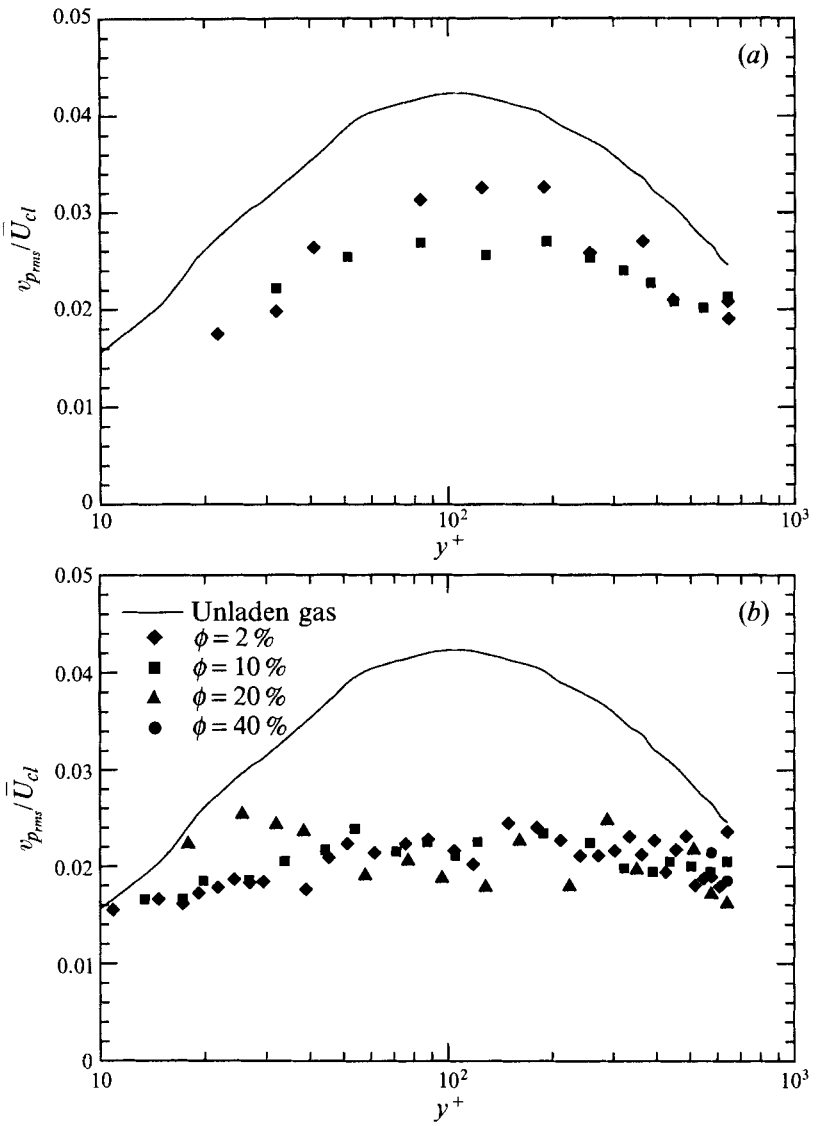

FIGURE 9. (*a*) 50 μm glass particle transverse fluctuation intensity profiles; (*b*) 70 μm copper particle transverse fluctuation intensity profiles.

variance in the direction normal to gravity. (The particle velocity standard deviations due to particle diameter variance are approximately 1%, 2% and 15% of the measured streamwise particle velocity standard deviations of 50 and 90 μm glass, and 70 μm copper particles, respectively.) Secondly, it is known that normal velocity fluctuations occur at higher frequencies than do streamwise fluctuations, to which frequencies particles are less able to respond (see figures 13 and 14). Furthermore, as Reeks (1977) showed, the spectrum of turbulence seen by a particle drifting through *isotropic* turbulence is shifted to higher frequencies in the direction normal to drift compared with the spectrum in the drift direction. And thirdly, there are no gradients in the gas-phase transverse mean velocity while there are gradients in the streamwise velocity. Since transversely migrating particles retain longer memories of their previous

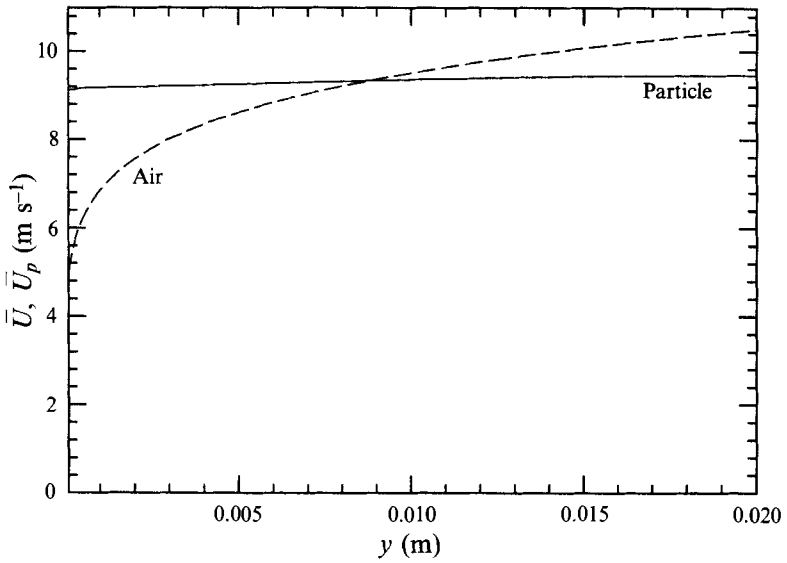

FIGURE 10. Simulation of 70 μm copper particle mean velocity profile.

streamwise velocity than do fluid particles, their streamwise fluctuation intensities are correspondingly greater (this effect is illustrated best by the aforementioned bimodal near-wall velocity PDFs).

While monodisperse particles in isotropic turbulence must have a fluctuation intensity smaller than the turbulence intensity, as Liljegren (1993) showed mean shear can elevate the fluctuation intensity over the turbulence intensity. The same mechanism – transverse mixing of streamwise particle momentum – accounts for the flat particle mean velocity profiles and negative slip velocities in the core flow. The measured transverse fluctuation intensity was used in a very simple model of particle motion, to explain the qualitative behaviour of the particle mean velocity. In this computation, a single particle was given a transverse velocity equal to the measured r.m.s. transverse velocity at the same distance from the wall. The particle started at the channel centreline, and moved towards one wall, from which it rebounded elastically. The particle streamwise velocity was determined by gravity and a linear drag law, with the steady fluid velocity field given by a $\frac{1}{7}$th power law. The resulting particle mean velocity profile – for 70 μm copper particles – is shown in figure 10. This crude representation of particle dynamics captures the essential features of the particle mean velocity: the profile is fairly flat, and particles lag the flow in the core and lead near the wall. The simulation's centreline slip velocity of 1 m s^{-1} is approximately that measured at a 0.1 mass loading, while the slip velocity at the wall is somewhat overpredicted. This simulation result is consistent with the large body of experimental results in pneumatic conveyance in pipes (§1.1). Moreover, the *streamwise* particle velocity fluctuation intensity that this simulation yields is roughly 0.2 m s^{-1}, or on the order of the measured fluctuations (cf. figure 7*b*).

3.2. *Turbulence modification*

Small particles at moderate mass loadings tend to reduce turbulence intensity, as mentioned in §1.1. The largest particles in these experiments were smaller than the Kolmogorov scale except near the wall where that scale is smallest, so they should satisfy most criteria for smallness. To investigate the dependence of turbulence

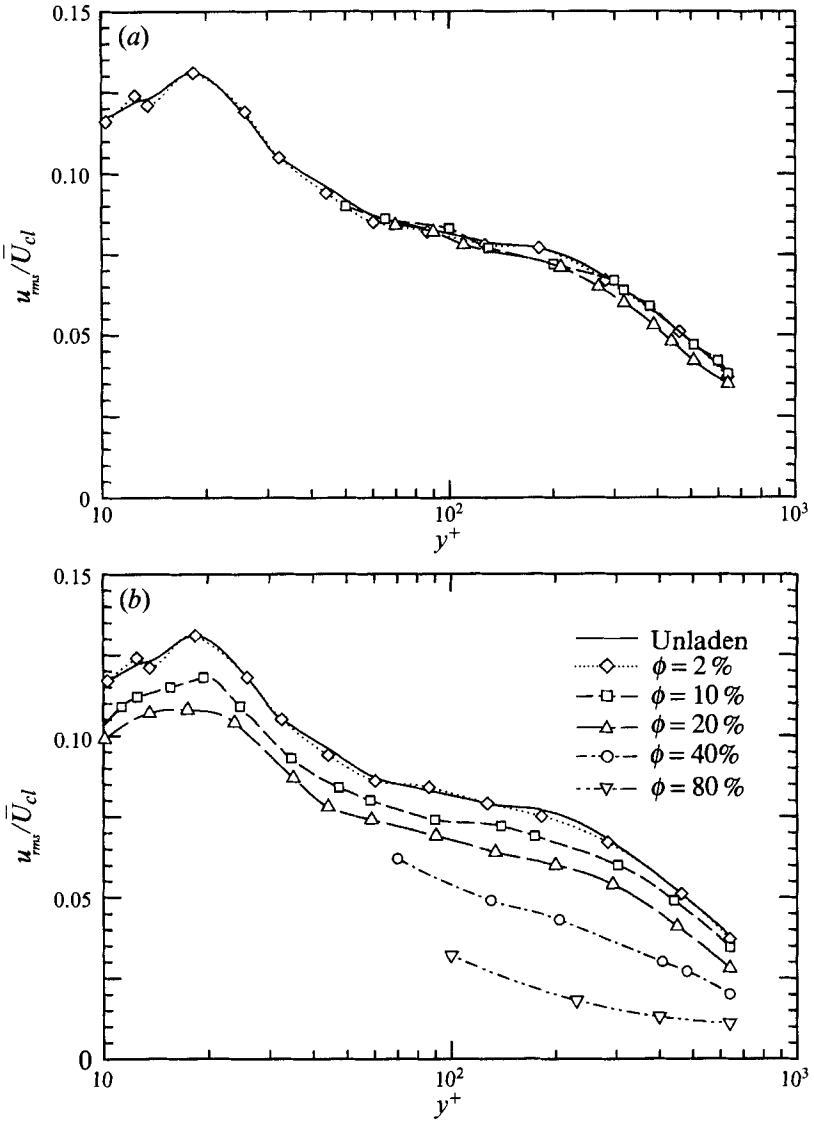

FIGURE 11. Streamwise turbulence intensity profiles in the presence of (*a*) 50 μm glass particles; (*b*) 70 μm copper particles.

attenuation on Stokes number and mass loading, gas-phase turbulence intensity profiles were measured at mass loadings up to 0.8.

3.2.1. *Gas-phase velocity measurements*

Profiles of streamwise turbulence intensity are shown in figures 11(*a*) and 11(*b*). In these and all following plots ϕ is the mass loading of particles defined as the global mass flow rate of particles normalized by the mass flow rate of air. The r.m.s. fluctuating velocity is normalized by the centreline streamwise mean velocity and is plotted against distance from the wall in wall units. The two most prominent trends are that the degree of turbulence attenuation increases with mass loading and with Stokes number. In figure 11(*a*), 50 μm glass particles are seen to have no effect on turbulence

at a mass loading of 0.1 and only a small effect at a mass loading of 0.2. The most massive particles, 70 μm copper, have a greater effect and reduced the turbulence intensity by 75% at the channel centreline. The sources of uncertainty in these measurements – primarily the variances in particle diameters – all tend to increase the variance of the measured velocity, so it is possible that turbulence attenuation was even more pronounced than these plots indicate. Estimated uncertainties in gas-phase turbulence intensity measurements range from 2% to 8%, with greater uncertainty at smaller Stokes numbers and higher mass loadings.

Again referring to figure 11, the degree of turbulence attenuation increases with increasing distance from the wall, albeit to a lesser extent than with variations in Stokes number or mass loading. In the case of 70 μm copper particles at 0.2 mass loading, for example, the reduction in turbulence intensity is 26% at the centreline, 17% at $y^+ = 100$, and 13% at $y^+ = 10$. This same trend was observed in pipe flow by Tsuji *et al.* (1984) and in a boundary layer by Rogers & Eaton (1991), and was ascribed variously to uneven drag loading, particle initial conditions, and particle–wall interactions. It was shown by figure 5 that gas-phase mean velocity profiles were essentially unmodified by the particles, so uneven drag loading is not likely to have been responsible; furthermore, particle initial conditions were nearly uniform and were unlikely to have had any persistent effects 300 half-widths downstream.

The turbulence kinetic energy budget differs strongly between the near-wall region, where production nearly balances viscous dissipation, and the outer region, where turbulent diffusion balances viscous dissipation. If the turbulence production mechanisms – instability waves rolling up into vortices – are not so strongly affected by particles as is diffusion of relatively inactive turbulence, then the increase in turbulence attenuation with distance from the wall might be explained. Experiments at high mass loadings in jets show little effect on the vortex roll-up process, suggesting that turbulence production is not strongly affected (see e.g. Longmire & Eaton 1990). Furthermore, the experiments of Rashidi, Hetsroni & Banerjee (1990) in horizontal water boundary layers show that small-diameter particles attenuate turbulence without modification of the frequency of turbulence-producing bursts. No measurements are available of the turbulent diffusion term in a particle-laden gas flow.

Turbulence attenuation in the transverse direction behaved in much the same manner as in the streamwise direction, as illustrated by the profiles in figures 12(*a*) and 12(*b*). (The apparent increase in turbulence intensity for the 0.02 mass loading of 50 μm glass particles is not understood, and may simply reflect the tendency of cumulative experimental uncertainty to increase measured velocity variances.) The 90 μm glass and 70 μm copper particles reduced turbulence intensity even at the lowest mass loading of 0.02.

The variation of transverse turbulence intensity with mass loading and distance from the wall differs in several respects from that in the streamwise direction. Although transverse turbulence attenuation is greater than streamwise attenuation at low mass loadings, it does not increase with mass loading to the same extent; for example, streamwise attenuation in the outer region at 0.4 mass loading of 70 μm copper particles is approximately twice that at a mass loading of 0.2, while the same ratio in the transverse direction is about 1.3. In the near-wall region, the location of maximum turbulence intensity moves towards the wall with increasing mass loading. Furthermore, the degree of turbulence attenuation decreases significantly as the wall is approached, and appears to tend towards zero, as was true for particle fluctuation intensities (figure 9).

Further insight into the nature of turbulence attenuation by particles is provided by

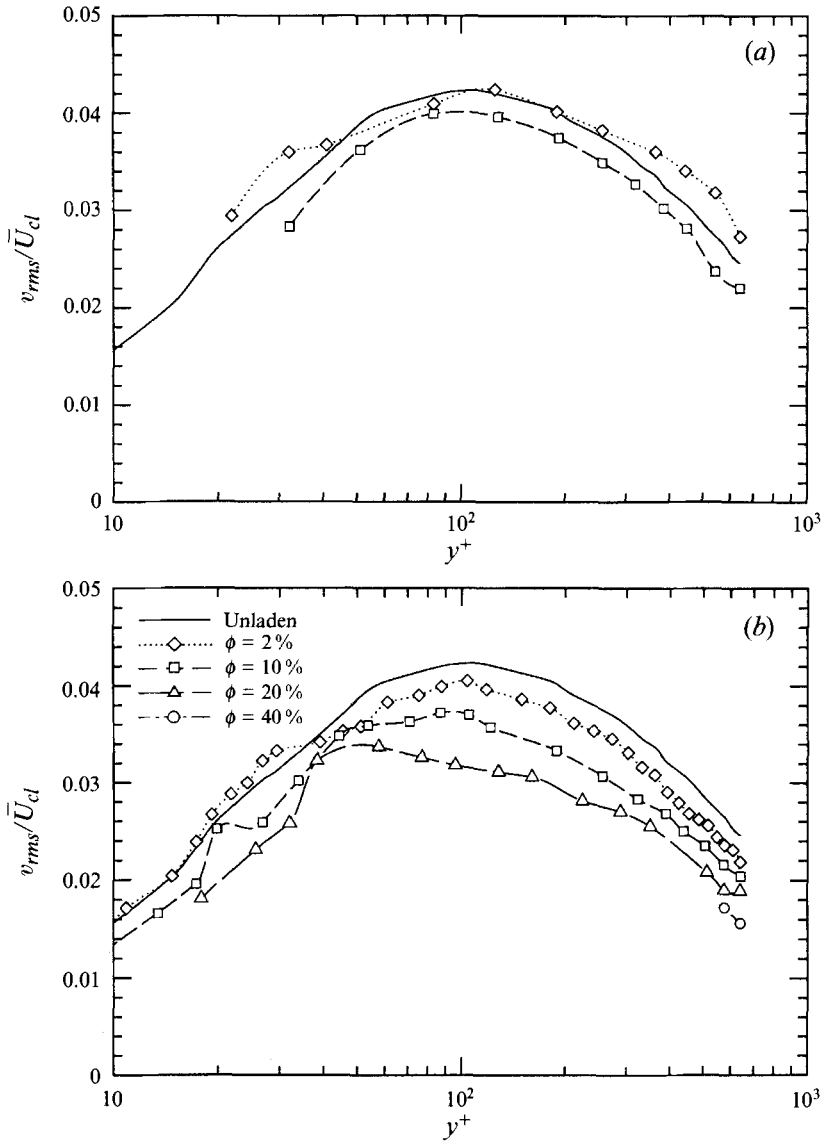

FIGURE 12. Transverse turbulence intensity profiles in the presence of (*a*) 50 μm glass particles; (*b*) 70 μm copper particles.

the flow power spectra in figure 13, measured at the centreline for various mass loadings of 70 μm copper particles. All of the spectra are normalized by $\overline{u^2}_{\phi=0}$, where ϕ is the particle mass loading, so that they reflect the true turbulence energy at each mass loading. Particles are seen to remove energy non-uniformly from the large scales (low frequencies) of the flow, and to augment the turbulence at high frequencies. It is not clear from these Eulerian measurements, however, that the extra energy at the high frequencies is manifesting itself as turbulence in the conventional sense. The extra measured energy at these frequencies could be due to many phenomena, including distortion of eddies causing energy transfer into higher harmonics, roll-up of particle wakes into eddies on this scale or simply measurement of similar flow fields in the vicinity of particles, passing at these frequencies. The increased energy at high

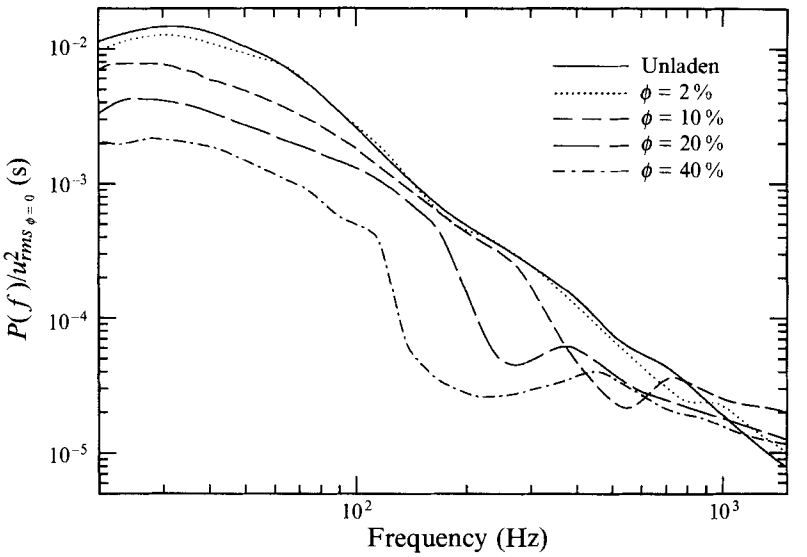

FIGURE 13. Streamwise velocity power spectra at the centreline in the presence of 70 μm copper particles.

frequencies is consistent with the experimental observations of Tsuji *et al.* (1984) and Rogers & Eaton (1991) as well as the computational work of Elghobashi & Truesdell (1993) and Squires & Eaton (1994). Rogers & Eaton postulated that the increased energy was associated with periodic measurement of similar flow fields around particles skirting the measurement volume at those frequencies. Squires & Eaton found the increased energy to be associated with the extra dissipation resulting from preferential concentration of particles into dense clusters. Elghobashi & Truesdell found that the particles are acting as localized sources of energy at high wavenumbers and as a result affect the cascade of turbulent energy across the spectrum. All of these investigations (and that of Squires & Eaton 1990*b*), however, found that particles removed energy uniformly from a broad range of scales. Each of the present spectra for mass loadings of 0.1, 0.2 and 0.4 has a pronounced dip, indicating that particles act on a preferred range of flow scales. Estimating the magnitude of the dip in each spectrum as the maximum value of the ratio of the power interpolated between the endpoints of the dip to the actual power, the magnitude is seen to increase with increasing mass loading; at 0.4 mass loading the power at the maximum dip is nearly one order of magnitude smaller than the interpolated value. The frequency at which the maximum dip occurs decreases with increasing mass loading. This trend suggests that at low mass loadings the extra dissipation due to particles acts on the same scales of the flow as does viscous dissipation, while at higher loadings the particles affect the larger scales. For the 0.4 mass-loading case the frequency of maximum attenuation is approximately 200 Hz, which corresponds to flow scales of approximately 2 mm, comparable with the Taylor microscale.

Although data rates for the laden flow were not sufficient for spectral measurements in the transverse direction, some insight might also be gained by comparison of the unladen-flow power spectra in the streamwise and transverse directions. Comparison of figures 13 and 14 shows that the energy in the transverse direction is contained at higher frequencies than for the streamwise direction. Heavy particles are less responsive to these high-frequency fluctuations, which results in lower transverse velocity

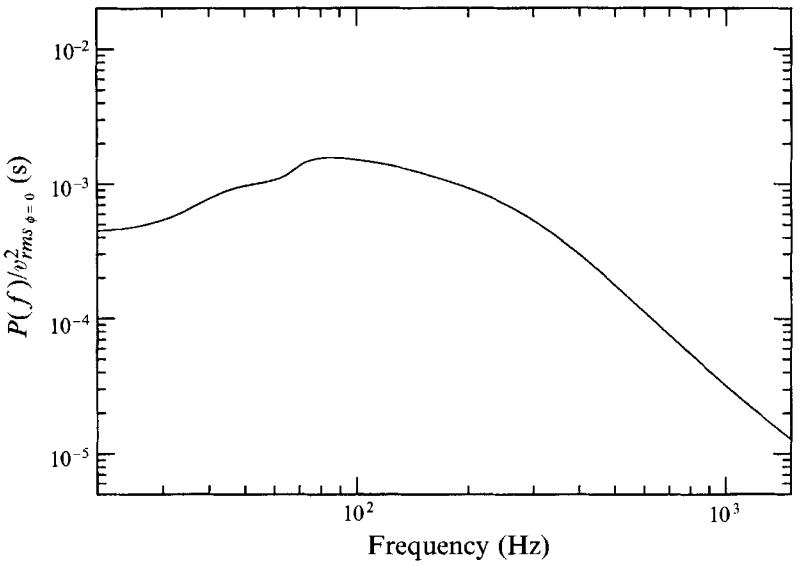

FIGURE 14. Transverse velocity power spectrum at the centreline (unladen flow).

fluctuations and perhaps explains the greater observed turbulence attenuation in the transverse direction.

3.2.2. *Comparison with model*

Considering the transport equation for turbulence kinetic energy, particles may be seen to act as an extra source of dissipation. For a flow with small particles – where a linear drag law may be applied – this equation is (Kulick *et al.* 1993)

$$\frac{\mathrm{d}k}{\mathrm{d}t} = \frac{\mathrm{d}k}{\mathrm{d}t}\bigg|_{sp} - \frac{\bar{C}}{\rho\tau_p}(\overline{u_i u_i} - \overline{u_i v_i}) - \frac{1}{\rho\tau_p}(\overline{cu_i u_i} - \overline{cu_i v_i}) - \frac{1}{\rho\tau_p}(\bar{U}_i - \bar{V}_i)\,\overline{cu_i}, \tag{3}$$

where lower-case symbols denote fluctuating quantities. In (3), the first term on the right-hand side represents the conventional k-equation for single-phase flows. The terms in this equation are modified indirectly by the presence of particles, and need to be accounted for. The remaining terms are lumped together as the extra dissipation due to particles, ϵ_p. The 70 μm copper particles are known to have a Poisson distribution in number density (see Kulick *et al.* 1993), so that the correlations involving the fluctuating particle number density, c, are small. Although the measured particle velocity fluctuation intensities were large at some locations, those values were not due to particle response to local fluctuations. Particle response to turbulence is approximated by (Pourahmadi & Humphrey 1983)

$$\overline{v_i v_i} = \frac{1}{1+St}\,\overline{u_i u_i}, \tag{4}$$

where the Stokes number is based on the fluid integral timescale as measured in the Lagrangian reference frame of a moving particle. Based on the computations of Squires & Eaton (1990*a*), it is estimated that the fluid integral timescale measured along the particle path is about one-half that measured in the classical Lagrangian reference frame, the 70 μm copper particles had a Stokes number of about 50 on this basis (Kulick *et al.* 1993), and so the fluid–particle velocity correlation $\overline{u_i v_i}$ was much

smaller than twice the turbulence kinetic energy $\overline{u_i u_i}$ in (3). The sole term that remains of the extra dissipation due to particles is then

$$\epsilon_p = \frac{\bar{C}}{\rho \tau_p} 2k, \tag{5}$$

which reduces to

$$\epsilon_p = \frac{2\phi}{\tau_p} k. \tag{6}$$

While (6) suggests that turbulence attention (owing to extra dissipation by particles) increases with decreasing Stokes number, contrary to this study's findings, it should be borne in mind that smaller-Stokes-number particles have large values of $\overline{u_i v_i}$ relative to $\overline{u_i u_i}$. For such particles the first term of ϵ_p in (3) will then be small. Furthermore, the terms in (3) that contain correlations with the fluctuating concentration may contribute to *reducing* the magnitude of ϵ_p; very little is known about the relative magnitudes of the constituent terms of (3) for small-St particles.

The relative importance of dissipation by particles as compared with viscous dissipation may be estimated by considering k–ϵ models for particle-laden turbulence. Rizk & Elghobashi (1989) were able to predict reasonably well the turbulence attenuation measurements of Maeda *et al.* (1989) and Tsuji *et al.* (1984) with a k–ϵ model, as were Rizk, Mostafa & Abolfadl (1993) the results of Rogers & Eaton (1991). Without solving the full model equations for the channel flow, we consider turbulence attenuation at the centreline. The turbulence kinetic energy and dissipation transport budgets are considerably simplified at the centreline of a fully developed channel, because the mean velocity gradient and first derivatives of k and ϵ are both zero (see, e.g. Mansour, Kim & Moin 1989 for the full transport budgets and single-phase k–ϵ model). In single-phase flow, turbulent diffusion of kinetic energy is exactly balanced by viscous dissipation. With the addition of dissipation by particles, the modelled form of the k-equation at the centreline becomes

$$\frac{\mathrm{d}k}{\mathrm{d}t} = C_\mu \frac{k^2}{\epsilon} \frac{\mathrm{d}^2 k}{\mathrm{d}y^2} - \epsilon - \epsilon_p = 0, \tag{7}$$

where $C_\mu k^2/\epsilon$ is the eddy viscosity. Similarly for dissipation, turbulent diffusion exactly balances viscous destruction in the single-phase case. Destruction of dissipation by particles is modelled analogously to viscous destruction (Elghobashi & Abou-Arab 1983), so the modelled ϵ-equation at the centreline is

$$\frac{\mathrm{d}\epsilon}{\mathrm{d}t} = \frac{C_\mu}{\sigma_\epsilon} \frac{k^2}{\epsilon} \frac{\mathrm{d}^2 \epsilon}{\mathrm{d}y^2} - C_{\epsilon_2} \frac{\epsilon}{k} \epsilon - C_{\epsilon_3} \frac{\epsilon}{k} \epsilon_p = 0. \tag{8}$$

For a given mass loading ϕ, let k/k_0 and ϵ/ϵ_0 be given by $\hat{k}_\phi$ and $\hat{\epsilon}_\phi$, respectively, where the zero-loading case is given by k_0 and ϵ_0. If second derivatives of k and ϵ (k'' and ϵ'', respectively) are assumed to scale with k and ϵ, respectively, then (7) and (8) may be written as

$$\hat{\epsilon}_\phi^2 + \frac{2\phi}{\tau_p} \frac{k_0}{\epsilon_0} \hat{k}_\phi \hat{\epsilon}_\phi - \hat{k}_\phi^3 = 0 \tag{9}$$

and

$$\hat{\epsilon}_\phi^2 + \frac{C_{\epsilon_3}}{C_{\epsilon_2}} \frac{2\phi}{\tau_p} \frac{k_0}{\epsilon_0} \hat{k}_\phi \hat{\epsilon}_\phi - \hat{k}_\phi^3 = 0, \tag{10}$$

respectively. In (9) and (10), (6) has been substituted for ϵ_p. The two equations differ

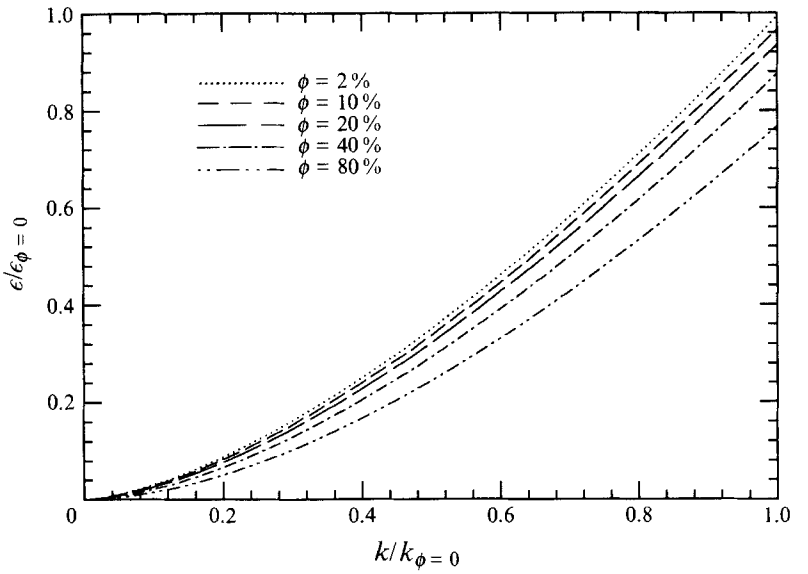

FIGURE 15. k–ϵ model variation of viscous dissipation with turbulence attenuation at channel centreline with 70 μm copper particles.

only in the ratio $C_{\epsilon_3}/C_{\epsilon_2}$ in the $\hat{\epsilon}$-equation, and there exist no unique non-zero solutions to these two equations; figure 15 shows a family of solution curves for $\hat{\epsilon}_\phi$ versus $\hat{k}_\phi$, with ϕ as the parameter, based on (9). Rizk & Elghobashi (1989) used $C_{\epsilon_2} = 1.8$ and $C_{\epsilon_3} = 2$, while Rizk *et al.* (1993) used $C_{\epsilon_2} = 1.8$ and $C_{\epsilon_3} = 1.7$, so in either case the solution curves should be very similar for either (9) or (10). Since this model has accurately predicted particle-laden pipe flow, where the same assumptions as made here could apply, the assumption that k''_ϕ and ϵ''_ϕ scale as k_ϕ and ϵ_ϕ must be in error. In fact, the experimental results from the channel and pipes show that k''_ϕ does *not* scale on k_ϕ.

Despite the absence of a unique analytical solution for k and ϵ, the curves of figure 21 may be used to estimate ϵ_ϕ given the experimental value of $\hat{k}_\phi$. (With $C_{\epsilon_3} \approx C_{\epsilon_2}$, as in Rizk *et al.* 1993, the values of ϵ_ϕ predicted by (9) and (10) differ by less than 2%.) Figure 16 shows the variation of $\hat{k}_\phi$, $\hat{\epsilon}_\phi$, and $\hat{\epsilon}_{p_\phi}$ with mass loading for the case of 70 μm copper particles at the centreline. In figure 16, $\hat{k}_\phi$ is determined from the measured values of $\overline{u^2}$ and $\overline{v^2}$ and the assumption that $\overline{w^2} = \overline{v^2}$; $\hat{\epsilon}_{p_\phi}$ is determined from (6) with $k = k_\phi$. Values of $\hat{\epsilon}_\phi$ are determined from (9). Also plotted in figure 16 are the same quantities for the $St = 1.50$ particles of Squires & Eaton (1990*a*), as well as $\hat{\epsilon}_\phi$ based on the computed value of k_ϕ and (9). Extra dissipation due to particles is nearly the same in the two different flows. Furthermore, despite its specificity to an inhomogeneous flow, (9) predicts the isotropic viscous dissipation reasonably well, which values are much larger than in the channel flow. The striking difference is in the degree of turbulence attenuation, which is much stronger in the channel flow than in isotropic turbulence.

There are, of course, manifold ways in which differences between low-Reynolds-number forced isotropic turbulence and high-Reynolds-number channel flow turbulence could account for the dramatically different amounts of turbulence attenuation with the same extra dissipation by particles. Perhaps particles interact more strongly with the mechanisms responsible for turbulent diffusion than with those for production, which also would serve to explain why turbulence attenuation is greater in the outer region than in the near-wall region. Even so, comparing the two flows is difficult;

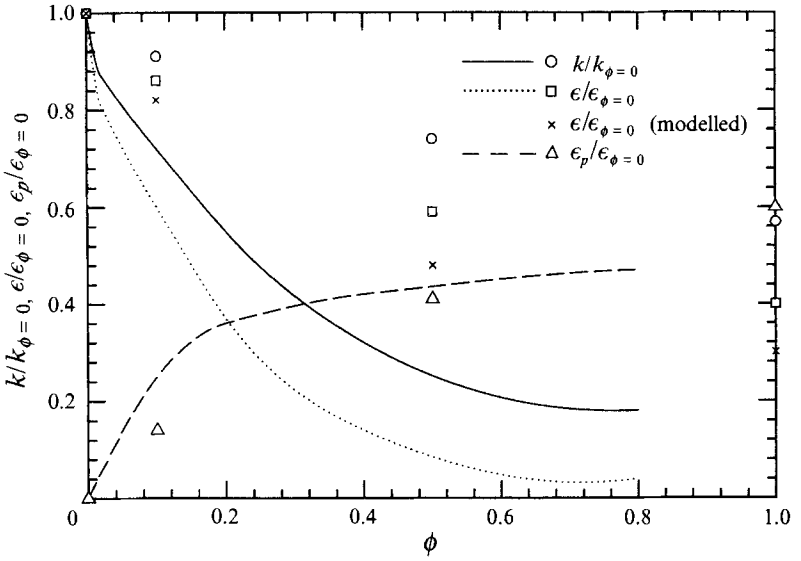

FIGURE 16. Variation with mass loading of turbulence kinetic energy, viscous dissipation and dissipation by particles. Curves are from channel centreline and symbols are from Squires & Eaton (1990*b*) isotropic turbulence.

although production and dissipation are in balance in both the isotropic turbulence computations and the buffer layer of the channel flow, production in the former case is by artificial isotropic forcing of the large scales – which remains unaffected by particles – while in the latter case production is generated by mean shear and Reynolds stresses. Only a few data are available from the buffer layer: at a 0.2 mass loading turbulence kinetic energy is attenuated by 35% at $y^+ = 20$, compared with reductions of 46% at the centreline and an estimated 14% in isotropic turbulence (see figure 16).

Neither is the difference in the dependence of turbulence attenuation on particle Stokes number clear. While Squires & Eaton (1990*a*) found that turbulence attenuation at a given mass loading depends only weakly on Stokes number – and even then in an inconsistent manner with mass loading variation – the current channel flow measurements exhibit a decided increase in turbulence attenuation with increasing Stokes number. These data and those from several other experiments are collected and displayed in figure 17, which shows the variation of *streamwise* turbulence attenuation with mass loading (attenuation in isotropic turbulence was isotropic, as well). The data fall roughly along two bands. The upper band (weak attenuation) includes only relatively light particles – plastic, glass, and small Stokes number computational particles. The lower band (strong attenuation) includes only heavy copper particles. More refined comparisons on the basis of particle relaxation time are difficult, as the definitions of Stokes number in dissimilar flows are not directly comparable. The experiments compiled in figure 17 occupy a narrow parameter space, leading to the banded nature of the turbulence attenuation. The three experimental configurations represented in the lower band, for instance, were all at similar flow Reynolds numbers and used similar particles. Additional experiments at different Reynolds numbers with different Stokes-number particles should, presumably, yield data that would fill in the domain between the two bands.

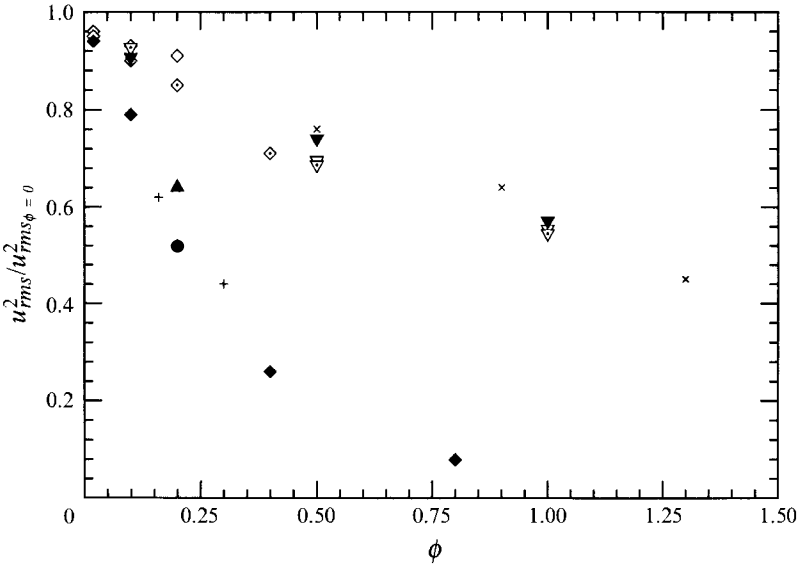

FIGURE 17. Attenuation of streamwise turbulent kinetic energy with mass loading variation: ×, Tsuji *et al.* (1984), 200 μm plastic particles – pipe centreline; +, Maeda *et al.* (1980): 93 μm copper particles – pipe centreline; ▽, ▽, ▼, Squires & Eaton (1990*b*); St = 0.52, 0.75, 1.5, isotropic turbulence DNS; ▲, Rogers & Eaton (1991): 70 μm copper particles – boundary-layer outer region. Present study: ◇, 50 μm glass; ◈, 90 μm glass; ◆, 70 μm copper particles, channel centreline.

4. Summary

Particle and fluid velocities have been measured in a turbulent channel flow, for three classes of spherical particles. It was shown that particle velocity profiles were relatively flat due to transverse mixing (in agreement with studies in round pipes), yet the fluid velocity profiles were unmodified. Particle velocity fluctuation intensities were found to exceed the turbulence intensity in the streamwise direction but were smaller in the transverse direction, due to the crossing-trajectories effect and different fluid velocity power spectra in the two directions.

The particles were found to attenuate turbulence, to an increasing degree as Stokes number, mass loading and distance from the wall were increased. Reductions in turbulence intensity were greater in the transverse than the streamwise direction, due primarily to the inability of the particles to respond well to the higher-frequency turbulent fluctuations in the transverse direction. In contrast to measurements in isotropic turbulence, streamwise velocity power spectra showed that turbulence was selectively attenuated in specific frequency bands. Despite the relatively small value of the extra dissipation due to particles compared with viscous dissipation, particles were much more effective at attenuating turbulence than in isotropic turbulence.

The authors should like to acknowledge the support of the National Science Foundation, which supported the first two authors with graduate fellowships and sponsored this research under grant number CTS-9005998-03.

REFERENCES

CSANADY, G. T. 1963 Turbulent diffusion of heavy particles in the atmosphere. *J. Atmos. Sci.* **21**, 222–225.

ELGHOBASHI, S. E. & ABOU-ARAB, T. W. 1983 A two-equation turbulence model for two-phase flows. *Phys. Fluids* **26**, 931–938.

ELGHOBASHI, S. E. & TRUESDELL, G. C. 1992 Direct simulation of particle dispersion in decaying isotropic turbulence. *J. Fluid Mech.* **242**, 655–700.

ELGHOBASHI, S. E. & TRUESDELL, G. C. 1993 On the two-way interaction between homogeneous turbulence and dispersed solid particles. I: Turbulence modification. *Phys. Fluids* A **5**, 1790–1801.

GASTER, M. & ROBERTS, J. B. 1977 The spectral analysis of randomly sampled records by direct transform. *Proc. R. Soc. Lond.* A **354**, 27–58.

GORE, R. A. & CROWE, C. T. 1991 Modulation of turbulence by a dispersed phase. *Trans. ASME* I: *J. Fluids Engng* **113**, 304–307.

KULICK, J. D., FESSLER, J. R. & EATON, J. K. 1993 On the interactions between particles and turbulence in a fully-developed channel flow in air. *Mech. Engng Rep.* MD-66. Stanford University.

LILJEGREN, L. M. 1993 The effect of a mean fluid velocity gradient on the streamwise velocity variance of a particle suspended in a turbulent flow. *Intl J. Multiphase Flow* **19**, 471–484.

LONGMIRE, E. K. & EATON, J. K. 1990 Structure and control of a particle-laden jet. *Mech. Engng Rep.* MD-58. Stanford University.

MAEDA, M., HISHIDA, K. & FURUTANI, T. 1980 Optical measurements of local gas and particle velocity in an upward flowing dilute gas-solids suspension. In *Proc. Polyphase Flow and Transport Technology*, pp. 211–216. Century 2-ETC, San Francisco.

MANSOUR, N. N., KIM, J. & MOIN, P. 1988 Reynolds-stress and dissipation-rate budgets in a turbulent channel flow. *J. Fluid Mech.* **194**, 15–44.

MANSOUR, N. N., KIM, J. & MOIN, P. 1989 Near-wall k–ϵ turbulence modeling. *AIAA J.* **27**, 1068–1073.

MAXEY, M. R. & RILEY, J. J. 1983 Equation of motion for a small rigid sphere in a nonuniform flow. *Phys. Fluids* **26**, 441–165.

POURAHMADI, F. & HUMPHREY, J. A. C. 1983 Modeling solid-fluid turbulent flows with applications to predicting erosive wear. *Phys.-Chem. Hydrodyn.* **4**, 191–219.

RASHIDI, M., HETSRONI, G. & BANERJEE, S. 1990 Particle-turbulence interaction in a boundary-layer. *Intl J. Multiphase Flow* **16**, 935–949.

REEKS, M. W. 1977 On the dispersion of small particles suspended in an isotropic turbulent fluid. *J. Fluid Mech.* **83**, 529–546.

RIZK, M. A. & ELGHOBASHI, S. E. 1985 The motion of a spherical particle suspended in a turbulent flow near a plane wall. *Phys. Fluids* **28**, 806–817.

RIZK, M. A. & ELGHOBASHI, S. E. 1989 A two-equation turbulence model for dispersed dilute confined two-phase flows. *Intl J. Multiphase Flow* **15**, 119–133.

RIZK, M. A., MOSTAFA, A. A. & ABOLFADL, M. A. 1993 Calculations of a particle-laden flat plate turbulent boundary layer. In *Gas-Solid Flows. ASME FED*-166 (ed. Stock *et al.*), pp. 169–175.

ROGERS, C. B. & EATON, J. K. 1991 The effect of small particles on fluid turbulence in a flat-plate, turbulent boundary layer in air. *Phys. Fluids* A **3**, 928–937.

SNYDER, W. H. & LUMLEY, J. L. 1971 Some measurements of particle velocity auto-correlation functions in a turbulent flow. *J. Fluid Mech.* **48**, 41–71.

SOMMERFELD, M. 1992 Modelling of particle-wall collisions in confined gas-particle flows. *Intl J. Multiphase Flow* **18**, 905–926.

SOO, S. L. 1956 Statistical properties of momentum transfer in two-phase flow. *Chem. Engng Sci.* **5**, 57–67.

SQUIRES, K. D. & EATON, J. K. 1990*a* The interaction of particles with homogeneous turbulence. *Mech. Engng Rep.* MD-55. Stanford University.

SQUIRES, K. D. & EATON, J. K. 1990*b* Particle response and turbulence modification in isotropic turbulence. *Phys. Fluids* A **2**, 1191–1203.

SQUIRES, K. D. & EATON, J. K. 1991 Measurements of particle dispersion obtained from direct numerical simulations of isotropic turbulence. *J. Fluid Mech.* **226**, 1–35.

SQUIRES, K. D. & EATON, J. K. 1994 Effect of selective modification of turbulence on two-equation models for particle-laden flows. *Trans. ASME* I: *J. Fluids Engng* (to appear).

TAYLOR, G. I. 1921 Diffusion by continuous movements. *Proc. Lond. Math. Soc.* A **20**, 196–211.

TCHEN, C. M. 1947 Mean value and correlation problems connected with the motion of small particles suspended in a turbulent fluid. PhD dissertation, University of Delft, The Hague.

TSUJI, Y., MORIKAWA, Y. & SHIOMI, H. 1984 LDV measurements of an air-solids two-phase flow in a horizontal pipe. *J. Fluid Mech.* **139**, 417–434.

WELLS, M. R. & STOCK, D. E. 1983 The effect of crossing trajectories on the dispersion of particles in a turbulent flow. *J. Fluid Mech.* **136**, 31–62.

YUDINE, M. I. 1959 Physical considerations on heavy particle diffusion. *Adv. Geophys.* **6**, 185–191.